Improving the Optical Properties of Self-Catalyzed GaN Microrods toward Whispering Gallery Mode Lasing

Christian Tessarek,*,†,‡ Robert Röder,§ Tom Michalsky,‖ Sebastian Geburt,§ Helena Franke,‖ Rüdiger Schmidt-Grund,‖ Martin Heilmann,† Björn Hoffmann,† Carsten Ronning,§ Marius Grundmann,‖ and Silke Christiansen†,⊥

†Max Planck Institute for the Science of Light, Günther-Scharowsky-Str. 1, 91058 Erlangen, Germany
§Institut für Festkörperphysik, Friedrich-Schiller-Universität Jena, Max-Wien-Platz 1, 07743 Jena, Germany
‖Institut für Experimentelle Physik II, Universität Leipzig, Linnéstr. 5, 04103 Leipzig, Germany
‡University Erlangen-Nuremberg, Institute of Optics, Information and Photonics, Staudtstr. 7/B2, 91058 Erlangen, Germany
⊥Helmholtz Centre Berlin for Materials and Energy, Hahn-Meitner Platz 1, 14109 Berlin, Germany

ABSTRACT: GaN microrods were grown self-catalyzed by a fast and simple metal–organic vapor phase epitaxy method without any processing before or after deposition. The prismatic microrods with a regular hexagonal cross-section, sharp edges, straight, and smooth sidewall facets act as a microresonator, as seen by the appearance of whispering gallery modes in the yellow defect band range. To improve their optical properties, a reduced Ga precursor flow is required during growth. However, their hexagonal microrod morphology is not maintained under these growth conditions.

The approach to start growth with a high Ga precursor flow and applying a ramp to a reduced precursor flow yield in significant enhancement of the near band edge emission in the upper part of the microrods. Whispering gallery modes in superposition with the near band edge emission can now be detected by cathodoluminescence measurements. These improvements lead to stimulated emission of a single whispering gallery mode up to ∼2 MW/cm² and multimode lasing with a threshold of 2.86 MW/cm² from an as-grown microrod under optical excitation at room temperature.

KEYWORDS: GaN, microrods, growth, MOVPE, whispering gallery modes, lasing
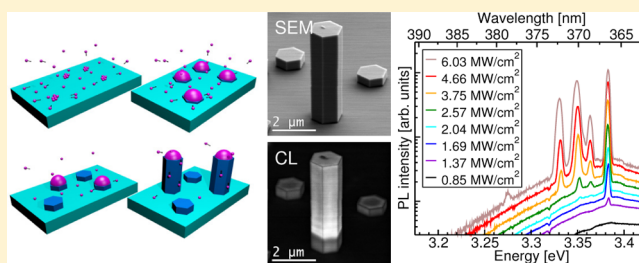
GaN laser diodes (LDs) are expected to be an alternative to light emitting diodes (LEDs) for solid state lighting since LDs are less affected by the "efficiency droop" at high current densities.[1] LDs can be based on GaN rod and wire structures, which have several advantages compared to two-dimensional (2D) GaN layers. High quality GaN material can be achieved in heteroepitaxy such as bottom-up growth of GaN nano- and microrods/-wires on inexpensive sapphire substrates.[2,3] Free-standing rods only suffer from strain-generated defects at the sapphire–GaN interface.[3,4] The relaxed upper part of the rods is nearly defect-free. A coalescence process typically leading to grain boundaries in 2D layers is also not required.[5] GaN rod structures are already applied in optoelectronics such as LEDs for the visible range but also as a basis for UV emission.[6−8] Stimulated emission under optical excitation has been observed in GaN nanowires; however, the fabrication is either time-consuming, needs complex processing before/after growth, and requires additional plasmonic or photonic crystal support.[9] GaN microrods can be used as microcavity resonators and whispering gallery modes (WGMs) with high quality (Q-) factors up to 4000 have already been demonstrated.[10] These Q-factors are comparable to complex fabricated GaN microdisk structures in which WGM lasing activity has been

reported.[11−15] However, the drawback of circular-shaped microdisk structures is the nondirectional light emission, whereas a hexagonal resonator benefits from directional out-coupling of light at the corners.[16] Compared to microdisks, the great technological advantage of the microrods is the short growth time of just 5−20 min without the need of additional growth and processing before or after microrod growth.[3,17,18] However, no lasing activity has been demonstrated in these kind of self-catalyzed GaN microrods. The potential of such microrods to be used as laser devices was hinted by another research group by the observation of whispering gallery modes in the strong and weak coupling regime.[19] For hexagonally shaped microrods based on the ZnO material system electrically driven WGM lasing has been demonstrated in combination with a p-type GaN layer.[20] It is expected that GaN microrods will also be a candidate to be used as whispering gallery mode laser diodes. The GaN microrods presented in our previous work suffer from low efficiency of the GaN near band edge (NBE) emission and WGMs are not observed in the NBE emission range.[10] It has already been presented that a reduced

trimethylgallium (TMGa; Ga precursor) flux improves the optical properties of GaN nanorods.[3]

In this study, possible optical modes in hexagonal resonators are discussed. The dispersion of the WGMs will clarify the observation of different Q-factors by either cathodo- or photoluminescence based on the measurement specifications. It will be shown that a low TMGa flux right from the start improves the optical properties, but without maintaining microrod morphology. Therefore, a combination of a high and low flux is applied leading to microrods with improved optical properties and optical modes are visible in the NBE emission range. Power-dependent optical excitation reveals stimulated emission of a single WGM and multimode lasing activity of a single microrod with improved optical quality.

■ EXPERIMENTAL SECTION

The GaN samples were grown on 2″ c-plane sapphire substrates utilizing an Aixtron 200RF horizontal flow metal−organic vapor phase epitaxy (MOVPE) reactor. TMGa, silane, hydrogen, and ammonia were used as precursors. Sapphire is nitridated at high temperature to form a thin AlN layer with N-polarity needed for rod growth.[21−23] Afterward, GaN is deposited for 5−20 min, supplying silane and adjusting a V/III ratio between 6−25. The presence of Si strongly enhances the vertical growth of GaN structures.[2,3,24,25] Due to the vapor−liquid−solid (VLS) growth and the low solubility of Si in the Ga droplet, Si is mainly incorporated as a SiN monolayer into the surface layer of the sidewalls of the rods leading to stabilized and antisurfactant m-plane facets supporting vertical growth.[25] All further details concerning growth can be found in ref 3. No further processing/preparation before or after growth is needed to obtain the microrods making the whole process cheap, fast and easy.

Scanning electron microscopy (SEM) and room temperature (RT) cathodoluminescence (CL) measurements were per-fomed utilizing a Hitachi S4800 in combination with a Gatan MonoCL setup. For the SEM images and CL measurements an acceleration voltage of 5 keV was used. A sample tilt of 60° between the surface normal and the electron beam was adjusted. Excitation dependent microphotoluminescence (μPL) experiments were performed on a single GaN microrod tilted by 22° with respect to its c-direction utilizing a pulsed Nd:YAG laser with an emission wavelength, pulse width, repetition rate, and spot size of 355 nm, 7 ns, 100 Hz, and ~1.5 μm^2, respectively. Angular resolved μPL measurements have been carried out using a pulsed Ti:sapphire laser with an emission wavelength, pulse width, repetition rate, and spot size of 264 nm, 2 ps, 76 Hz, and ~5 μm^2, respectively. The sample was tilted by 90° with respect to the surface normal, that is, excitation and detection was performed perpendicular to the c-direction of the microrods. The PL emission of the samples was collected by a high numerical aperture (NA = 0.4) UV microscope objective allowing to detect an angular range of about ±23°. By imaging the back focal plane of the objective on a monochromator entrance slit it was possible to image the optical mode dispersion directly on a CCD array chip.

■ RESULTS AND DISCUSSION

Optical Modes in Hexagonal Resonators. It has already been shown that WGMs appear in regular hexagonal shaped GaN microrods.[3,10,18,26] However, beside the hexagonal WGMs also occurrence of Fabry−Perot (FP) and triangular WGMs

(also known as quasi-WGMs) was reported in this kind of geometry.[27,28] As a basis for further discussion a short overview over some possible optical modes and their properties will be carried out.

In Figure 1 the photon energy dependent refractive index of GaN n_{GaN} from ref 29 is plotted (blue graph, left axis). The
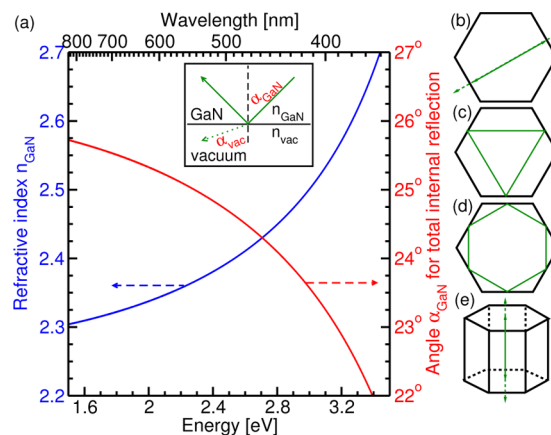
Figure 1. (a) Refractive index of GaN and the criticle angle of incidence for total internal reflection. The schemes (b−e) depict possible optical modes in a hexagonal geometry.

angle of incidence α_{GaN} (see inset for definition) for total internal reflection ($\alpha_{vac} = 90°$) of a light beam in the GaN crystal without a surrounding medium ($n_{vac} = 1$) can be calculated using Snell's law of refraction and is plotted in Figure 1 (red graph, right axis). In the considered wavelength range, all light with an angle of incidence larger than ~26° (25.5° for NIR and 22° for UV) is totally internal reflected.

The schemes in Figure 1b−e show possible modes in a hexagonal geometry. FP modes have to be considered between two opposite sidewall facets (b). However, large losses of light are present since only 17% of light (at λ = 500 nm) is reflected yielding low Q-factors of ~10 for a microrod with a diameter d = 2 μm using $Q = 2\pi d n_{GaN}(R_1 R_2)^{1/2}/\lambda(1 - R_1 R_2)$ (R_1 and R_2 are the reflectivities of the facets).[30]

For triangular WGMs with $\alpha_{GaN} = 30°$ (c) and hexagonal WGMs with $\alpha_{GaN} = 60°$ (d) total internal reflection occurs. Both types of modes are quite stable and high Q-factor WGMs can be expected depending on the diameter and on the shape of the corners. Finally, in a microrod with a flat top facet also top-bottom FP oscillations are probable. However, similar to the planar case there are only low Q-factors of ~22 expected for a microrod with a length of 10 μm due to strong losses of light at the GaN-sapphire interface (R = 4%).

Influence of the Ga Precursor Flow on the Morpho-logical and Optical Properties of GaN Microrods. Microrods with high morphological quality showing high quality WGMs but with rather weak optical properties in terms of weak GaN NBE emission and strong yellow defect luminescence have been reported in ref 10. It was shown in ref 3 that a reduced Ga precursor flow improves the optical properties of GaN nanorods. This section will show problems and advantages for a reduced Ga precursor flow applied for microrod growth. The results will lead to a two-step approach presented in the next section to improve the optical properties of GaN microrods finally leading to WGM lasing.

Three samples have been grown with different TMGa (Ga precursor) fluxes: 40 sccm for 5 min, 20 sccm for 10 min, and

10 sccm for 20 min, that is, the total amount of supplied material is constant for each sample. The SEM images are shown in Figures 2a−c. With 40 sccm, vertically aligned GaN
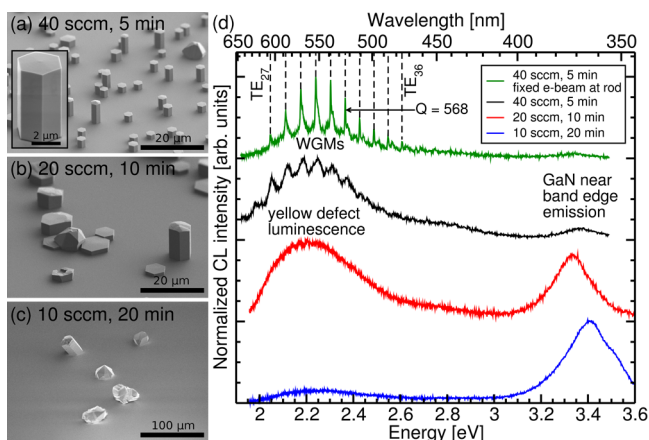
Figure 2. SEM images of GaN samples grown with (a) 40 sccm, (b) 20 sccm and (c) 10 sccm for 5, 10, and 20 min, respectively. Please note the different scale bar for image (c). The graph (d) summarizes the RT CL spectra recorded for each sample. The black, red, and blue spectra are taken from an ensemble. The green spectrum is recorded with a fixed electron beam (e-beam) during the CL measurement at the sidewall facet of the microrod (detailed view in the inset of (a)). The black dashed lines are the calculated TE triangular WGMs.

microrods with mostly regular hexagonal cross-section, smooth and straight sidewall/top facets, and sharp edges have formed on the sapphire substrate. Reducing the TMGa flux to 20 sccm leads to lower density of GaN structures. The regular hexagonal cross-section is not maintained and most of the top surfaces exhibit an unevenly random structure. A further reduction of the flux to 10 sccm disables microrod growth.

The VLS growth mode is expected to be responsible for the morphological changes of the samples with different Ga precursor fluxes shown in Figures 2a−c. Starting with a high Ga precursor flow leads to spontaneous formation of Ga droplets on the surface and microrod growth is enabled. Reducing the TMGa flux has two effects: First, the V/III ratio is increased and the growth regime is shifted toward a vapor−solid growth mode typical for lateral 2D layer growth by MOVPE.[17,31] Second, the ability to form Ga droplets is reduced since the growth takes place in a strong etching regime due to the high temperature and the H_2 atmosphere leading to a low density of Ga atoms on the surface. Therefore, at low fluxes no Ga droplet formation takes place on the bare sapphire substrate without nucleation sites, thus GaN microrod growth is disabled. This is in contrast to the nanorod growth. In order to obtain nanorods, a GaN nucleation layer has to be deposited (prior to nanorod growth) leading to the formation of small GaN flakes.[3] Ga atoms accumulate at these flakes promoting Ga droplet formation. Nanorods can be grown at even lower fluxes of 5 sccm.[3] It is concluded that the microrod growth first has to be initiated applying a high Ga precursor flux.

Respective CL measurements of the samples taken at RT are shown in Figure 2d. For the sample grown with 40 sccm, the yellow defect band dominates and only weak NBE emission can be detected. Furthermore, an additional emission band appears around 450 nm, which might be attributed to surface related emission.[32] Reducing the TMGa flux to 20 sccm increases the NBE emission. A further decrease to 10 sccm leads to

dominating GaN NBE emission in the spectra. The CL results on microrods show a similar trend, which was already observed for GaN nanorods.[3]

With a fixed electron beam at the sidewall facet of a single microrod of sample (a) optical modes appear in the CL spectra in superposition to the yellow defect luminescence (green graph in Figure 2). For the interpretation of the modes, in previous publications the best agreement was achieved assuming hexagonal WGMs and an isotropic refractive index reduced by 10−15%.[3,10,18,26] In the present paper a carrier-induced modification of the refractive index was included in the calculations based on the plane wave model (interference of a light wave with itself after a complete circulation in the resonator).[33,34] For this particular microrod a high doping concentration of 1.7×10^{20} cm^{-3} was assumed in agreement with other reports on this kind of rod.[10,35] In principle, due to the birefringence effect, an ordinary and extraordinary refractive index for transversal electric (TE) and transversal magnetic (TM) polarization, respectively, should be used for the simulation of the WGMs. However, to the best of the authors' knowledge, up to now no proper extra-/ordinary refractive index can be found in the literature. Ordinary and extraordinary refractive indexes are either only determined for the infrared to visible (>400 nm) spectral range[36−39] or show strong deviation from commonly used refractive indexes.[27,40] Therefore, here it was decided to use a commonly accepted refractive index from ref 29 that can be used in the UV (close to GaN NBE emission) and visible spectral range as an ordinary refractive index for TE polarized WGMs. The diameter was set to 2.848 μm, which is in good agreement with the diameter of 2.84 μm determined via SEM. Assuming triangular TE WGMs almost perfect agreement between measurement (green graph) and simulation (black dashed lines) was obtained. It is not clear why triangular WGMs are observed rather than hexagonal WGMs. It might be possible that some sidewall facets are slightly tilted with respect to the m-plane or are damaged/rough for the investigated microrod. In such a case, a hexagonal WGM is not stable in contrast to a triangular WGM.[28,41] A Q-factor of 568 was determined for the TE WGM with mode number 33.

It was shown that the yellow defect luminescence band is quite useful to classify WGMs. Since no lasing was shown from the defect band up to now, it is desired to improve the NBE emission and decrease the defect band contribution. For the samples discussed in Figure 2 no modes are observed in the NBE emission range due to low intensity.

Improving the Optical Properties of GaN Microrods. The approach to improve the optical properties without losing the microrod morphology is to start with a high TMGa flux and to change to a lower TMGa flux during growth. A sample was grown with a starting flow of 40 sccm TMGa for 20 s; during the following 50 s the flux was gradually reduced to 10 sccm, and further growth was carried out for 1040 s.

The SEM images, the corresponding pan- and monochromatic CL maps and CL spectra of such a sample with a variation of the TMGa flux are shown in Figure 3. The microrod morphology is maintained, as shown in the SEM images in Figure 3a,e. Basically two types of rods have formed: microrods or -disks with a reduced height and microrods with an increased height up to ~10 μm. The diameter of the structures is 1.2−2 μm.
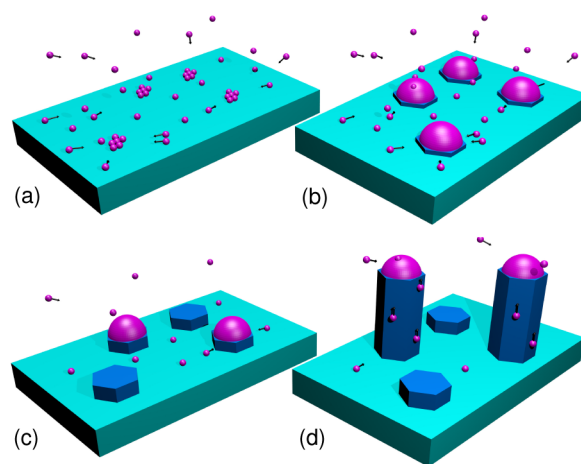
The situation during growth for such a sample with a variation in the TMGa flux is schematically depicted in Figure 4. The high TMGa flux of 40 sccm at the beginning of the
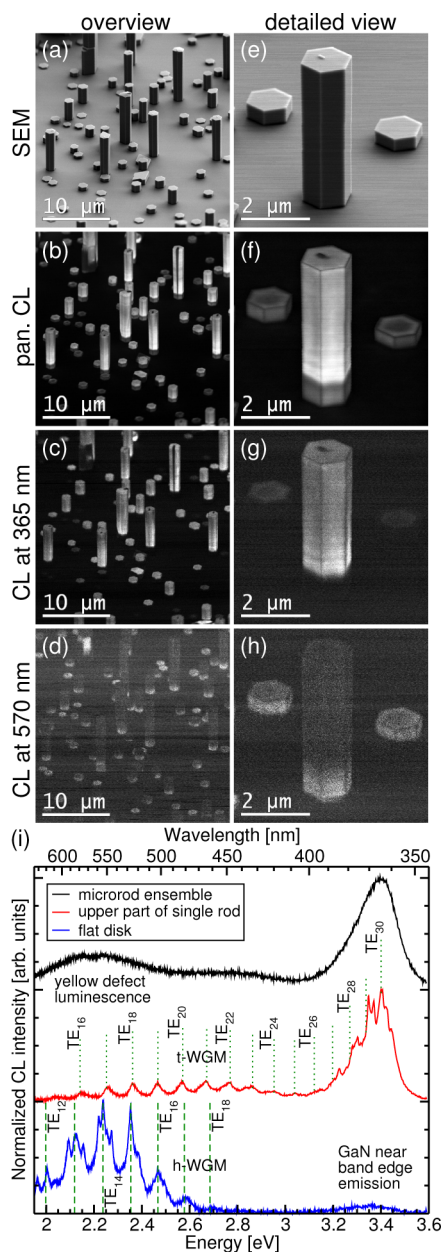
Figure 3. Overview of an ensemble of microrods and a detailed view of a single microrod is presented: (a, e) SEM images; (b, f) panchromatic CL map; (c, g and d, h) monochromatic CL map at 365 and 570 nm, respectively. The small pyramid/black spot on top of the microrods is known as the top of an inversion domain with Ga polarity.[3] In graph (i) the normalized CL spectra are shown and shifted for clarity. The black graph was recorded while scanning an ensemble of microrods. The red and blue graphs were recorded with a fixed electron beam directed to the sidewall of the upper part of the long single microrod and to a flat disk shown in (e), respectively. For the red and blue graph, the green dotted and dashed lines are the calculated TE triangular (t-)WGMs and TE hexagonal (h-) WGMs, respectively.

growth leads to a high density of Ga atoms on the sapphire surface and thus to Ga accumulation (Figure 4a). Spontaneous Ga droplet formation is initiated and therefore microrod growth is enabled (Figure 4b). All droplets are stable due to the high TMGa flux. The change in the flux to 10 sccm leads to the disappearance of some of the droplets on top of the microrods due to consumption (transformation into GaN), desorption at high temperature or shrinking due to Ostwald ripening (Figure

Figure 4. Scheme depicts the situation during growth for the sample with a variation in the TMGa flux (cf. Figure 3). (a, b and c, d) High and low TMGa flow, respectively. The cyan platforms, the small violet spheres, the large violet hemispheres, and the blue hexagons represent the sapphire substrate, Ga atoms, Ga droplets, and the GaN microrods, respectively. For simplicity, N and Si atoms are not sketched.

4c).[42] Not depicted in the scheme is the formation of a SiN layer on the sapphire surface and on the m-plane facets, enhancing vertical growth due to an antisurfactant and stabilizing effect in accordance with the findings in ref 25. Microrods without a droplet stop growing and an additional SiN layer forms on top of the microrod preventing further growth due to the antisurfactant effect and desorption due to the higher thermal stability of the SiN layer compared to GaN.[25] Only a reduced number of microrods grow further, because a Ga droplet on the top of a microrod is supplied with a sufficient amount of new material (Figure 4d).

The black graph in Figure 3i represents the RT CL spectrum of an ensemble of microrods. The spectrum is quite similar to the blue spectrum from Figure 2d. The NBE emission dominates and there is only weak contribution of the yellow defect luminescence. The panchromatic CL maps in (b) and (f) reveal that the upper part is of higher optical activity than the basis of the microrods. The NBE emission is only excited if the electron beam scans the upper part of the microrods as can be seen in the monochromatic CL maps recorded at 365 nm. The monochromatic CL map taken at 570 nm shows the presence of the yellow defect luminescence along the entire microrods but with a maximum intensity at the basis. The red and blue spectra in graph (i) recorded with a fixed electron beam directed to the upper part of the microrod and to a flat disk, respectively, coincide with the monochromatic CL maps. The basis of the microrods shows the same optical properties as the flat disks. The difference in the optical properties between basis and upper part of the microrod can be explained by the different TMGa fluxes applied during growth similar to the results shown in Figure 2: a high TMGa flux at the beginning of the microrod growth leads to weak NBE emission activity, whereas a low TMGa flux significantly enhances the NBE emission.

WGMs are visible in the CL spectra of GaN microrods grown using the optimized parameters as described above (see red and blue graph in Figure 3). The Q-factor of the modes is lower due to the reduced diameter compared to the microrods discussed in Figure 2. However, WGMs can now also be detected superimposed to the NBE emission (see red graph in

Figure 3). The best agreement between experiment and simulation for the microrod with a measured diameter of 1.70 μm was obtained by assuming TE triangular WGMs. An inner diameter of 1.649 μm, a carrier concentration of 2.3 × 10^{20} cm^{-3} and mode numbers 16−30 for TE WGMs were used for the calculations. However, at the NBE emission the sequence of modes is quite complicated and poor agreement is achieved. Due to the large variety of different refractive indexes for GaN, which can be found in the literature,[27,36−40] it is obvious that the refractive index used in the present study, proposed by ref 29, might not be ideal for the complete spectrum from a GaN microrod. Further modes are present at the NBE emission that can not be explained by TE triangular WGMs, but might be attributed to TM triangular or TE/TM hexagonal WGMs. The results show that the growth approach is reasonable and microrods are obtained with improved optical properties and WGMs are visible in the NBE emission range.

For a microdisk there is only weak NBE emission as visible in the blue graph of Figure 3, because the disk was grown with a high TMGa flux and stopped growing after switching to lower TMGa flux. For a microdisk with a measured diameter of 1.38 μm also modes appear in superposition to the yellow defect luminescence. For this particular microdisk, the best agreement was obtained assuming TE hexagonal WGMs. An inner diameter of 1.313 μm, a carrier concentration of 1 × 10^{20} cm^{-3}, and mode numbers from 12−18 were used for the calculations. From the present point of view it is not clear why sometimes hexagonal or triangular and TM or TE modes are observed. Polarization dependent optical experiments with a detailed view on the size and form of the microrod/disk will be carried out in the future to clarify this query.

The physical reason for the enhancement of the NBE emission is still under discussion. The V/III ratio and the Si doping concentration (for constant TMGa flux) was not found to have such a strong influence on the NBE emission. It is assumed that the dependence of the NBE emission on the TMGa flux is caused by the density of Ga atoms on the surface. A higher density of Ga atoms might influence the surface mobility of N and Si. Hence, less N and Si can reach the droplet on top of the microrod. The absence of N might lead to defect generation in the GaN microrod, which act as nonradiative recombination centers reducing the NBE emission. Furthermore, a lower mobility of N would enhance the resting time of N on the surface, which leads to higher probability of N_2 formation, further reducing the N concentration on the surface and thus in the droplet.

**Angular Resolved Microphotoluminescence Measurements.** By different experimental techniques different values for the Q-factors were obtained. For CL investigations a Q-factor of ~5 × 10^2 was found whereas a Q of ~4 × 10^3 is observed by means of microphotoluminescence (μPL), that is, there is a difference of 1 order of magnitude.[10] In Figure 5a the angular dispersion of the WGMs from a GaN microrod with improved optical properties is shown. With increasing angle there is a blueshift of the WGMs. The impact of the dispersion on the Q-factor is shown in Figure 5b. Sharp WGMs are visible in the spectra recorded at Θ = 0. The WGM at 2.12 eV has a Q-factor of 244. The spectrum which depicts the detected microrod emission integrated from Θ = −20° to +20° shows slightly blue-shifted (~2 meV) and broadened modes. The Q-factor of the WGM at 2.12 eV is reduced to 133. The mirror in the CL setup collects almost all the luminescence emitted in the upper hemisphere (Θ = ~−90° to ~+90°) leading to larger full
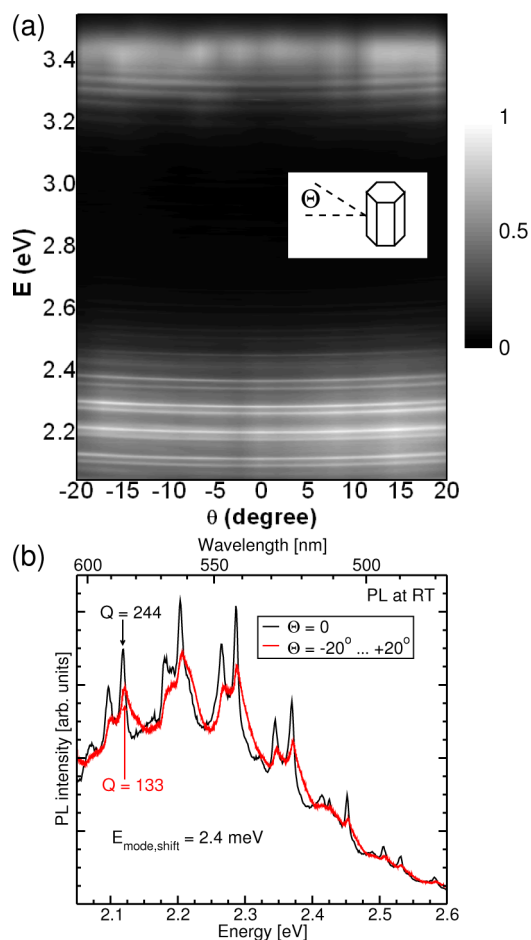
Figure 5. (a) 2D map of the angular dispersion of the WGMs in superposition with the NBE emission and the yellow defect luminescence. The inset defines the angle Θ with respect to the microrod orientation. The graph in (b) shows the yellow defect band of two spectra recorded at Θ = 0° and integrated from Θ = −20° to +20°. The double peaks appearing in the angular resolved μPL spectra within the spectral range of the yellow defect luminescence belong to the splitting of TE and TM modes. This is a consequence of the different phase shifts for the two polarizations during the total internal reflection according to the Fresnel equations.[43]

widths at half-maximum (FWHM) and therefore to WGMs with decreased Q-factors. In standard (not angular resolved) μPL measurements, depending on the numerical aperture, only a cone is detected, that is, the angular range is smaller than in CL investigations and thus higher and more realistic Q-factors are obtained.

WGM Lasing in GaN Microrods. Excitation power dependent μPL measurements have been performed on a single GaN microrod with improved optical properties and are presented in Figure 6. Up to an excitation power of 1 MW/cm^2, only the NBE emission is visible. At ~1.37 MW/cm^2 a single emission mode appears at 3.384 eV. Stimulated emission of the single mode can be observed up to 2 MW/cm^2. Figure 6b shows a linear plot of the integrated intensity against the excitation power up to 2 MW/cm^2, which allows to roughly estimate the onset of the stimulated emission at P_{on} ~ 1.1−1.2 MW/cm^2. The plotted FWHM show significant line width narrowing above onset. Above 2 MW/cm^2 two further modes appear at 3.349 and 3.364 eV. Further increasing the excitation
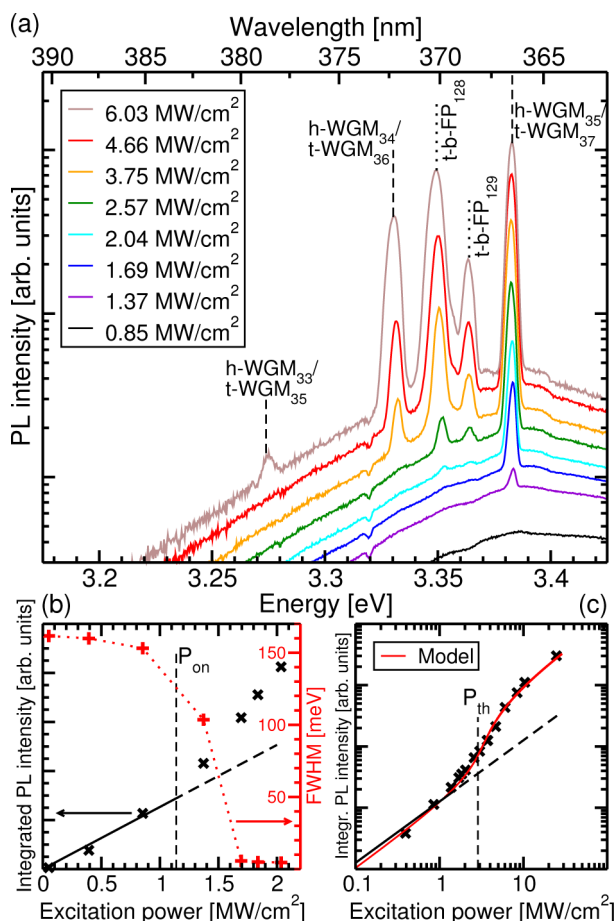
Figure 6. (a) Excitation power density dependent μPL spectra recorded at RT on a single GaN microrod. The dashed lines correspond to calculated triangular (t-)WGMs or hexagonal (h-)WGMs, the dotted lines mark the position of top-bottom (t-b) FP modes. Graph (b) shows the linear plot of the integrated PL intensity vs excitation power density up to 2 MW/cm^2 with an estimated onset of stimulated emission P_{on} at 1.1−1.2 MW/cm^2 (black symbols, left axis). Stimulated emission of the single WGM can be observed up to 2 MW/cm^2. The right axis displayed in red color and the red symbols correspond to the FWHM of each spectra. The straight, dashed, and dotted lines are guides to the eye. Graph (c) shows the double logarithmic plot of the integrated intensity vs excitation power density with a lasing threshold P_{th} at 2.86 MW/cm^2. From the model, a spontaneous-emission coupling factor of $\beta = 0.08$ is determined.

power up to 6 MW/cm^2 leads to additional modes at 3.331 eV and at 3.275 eV.

The double logarithmic plot for the entire excitation power range applied in Figure 6c follows the characteristic s-shaped course of a multimode laser oscillator.[44,45] The linear slope below 1 MW/cm^2, indicating the spontaneous emission regime converts to the superlinear increase of amplified spontaneous emission above ∼1.2 MW/cm^2, which is again followed by a linear slope for the excitation power increase above 10 MW/cm^2 proving lasing. From fitting of the experimental data with a multimode laser model, the threshold for lasing and the spontaneous-emission coupling factor was obtained with a value of $P_{th} = 2.86$ MW/cm^2 and $\beta = 0.08$, respectively.[46]

The exact height and diameter of the microrod can not be determined from the optical image of the μPL setup. It was also not possible to measure the microrod size afterward in an SEM because the microrod was destroyed due to the high power of

the excitation laser. Therefore, it is not obvious to specify the nature of the modes. Nevertheless, an estimation is performed based on the fact that WGMs from this kind of microrods are observed (see Figures 2d and Figure 3i and refs 3, 10, 18, and 26 and that most of the long microrods have an inner diameter between 1.5−2 μm and a height up to 10 μm, as obtained from SEM investigations. Calculations have been performed either considering hexagonal WGMs (TE, inner diameter 1.749 μm, carrier concentration 2×10^{20} cm^{-3}, mode number 33−35) or triangular WGMs (TE, inner diameter 2.037 μm, carrier concentration 2×10^{20} cm^{-3}, mode number 35−37) and are depicted as dashed lines in Figure 6a. Good agreement between calculated and measured modes is achieved. The modes at 3.384 eV, 3.331 and 3.275 eV seem to be of whispering gallery type. The other two modes at 3.349 and 3.364 eV can be calculated assuming top-bottom FP oscillations (microrod height 9.008 μm, carrier concentration 1×10^{20} cm^{-3}, mode number 128−129).

The onset of stimulated emission at 1.14 MW/cm^2 of the WGM at 3.384 eV and the lasing threshold of 2.86 MW/cm^2 for this particular microrod is quite high compared to other reports on WGM lasing in GaN microdisks and FP lasing in GaN nanowires.[9,12−15] This has several reasons: the Q-factor in a hexagonal system is basically lower compared to a circular disk. There is no optical confinement in vertical direction compared to a freestanding disk. The small diameter of the microrods also causes lower Q-factors.[27,34,47] For top-bottom FP modes there are strong losses at the sapphire/GaN interface. A reduction of the WGM lasing threshold is expected for increasing the diameter of the microrods. A better vertical confinement of the modes can be achieved by the growth of axially arranged high index cladding layers (e.g., axial AlGaN/GaN/AlGaN rod) or the growth of rods with sections having different diameters.[48] Higher optical activity is expected for InGaN quantum wells or dots deposited on the microrods.

A reduction of the diameter leads to spectrally well separated WGMs.[26] Whispering gallery single mode operation should therefore be enhanced if the diameter is further decreased, however, to the expense of the lasing threshold. If the rod diameter is too small, WGM lasing might be suppressed completely due to low Q-factor and top-bottom FP modes would dominate the lasing spectra. Suppression of the FP modes should be achieved if the top surface is structured, that is, scattering rather than reflection takes place. The structuring can be performed by reactive ion etching without any damage to the sidewall facets.[25]

In comparison to other materials, such as ZnO with similar hexagonal geometry, showing WGM lasing below 100 kW/cm^2, it becomes clear that there is still room for improvement concerning the optical quality of the GaN microrods.[16]

■ CONCLUSIONS

A reduction of the TMGa flux improves the optical properties in terms of enhanced NBE emission but disables microrod growth. A combination of a high TMGa flux at the growth start and a ramp to a lower TMGa flux maintains microrod growth and significantly improves the NBE emission, as shown in spatially resolved CL measurements. WGMs are observed in the NBE emission range and excitation dependent μPL studies show stimulated emission of a single WGM in a range between 1.1−2 MW/cm^2. The threshold for multimode lasing appears at 2.86 MW/cm^2.

■ AUTHOR INFORMATION

Corresponding Author
*E-mail: christian.tessarek@mpl.mpg.de.

Notes
The authors declare no competing financial interest.

■ REFERENCES

(1) Wierer, J. J.; Tsao, J. Y.; Sizov, D. S. Comparison between Blue Lasers and Light-Emitting Diodes for Future Solid-State Lighting. *Laser Photonics Rev.* **2013**, *7*, 963−993.

(2) Koester, R.; Hwang, J. S.; Durand, C.; Le Si Dang, D.; Eymery, J. Self-Assembled Growth of Catalyst-Free GaN Wires by Metal-Organic Vapor Phase Epitaxy. *Nanotechnology* **2010**, *21*, 015602.

(3) Tessarek, C.; Bashouti, M.; Heilmann, M.; Dieker, C.; Knoke, I.; Spiecker, E.; Christiansen, S. Controlling Morphology and Optical Properties of Self-Catalyzed, Mask-Free GaN Rods and Nanorods by Metal-Organic Vapor Phase Epitaxy. *J. Appl. Phys.* **2013**, *114*, 144304.

(4) Hersee, S. D.; Rishinaramangalam, A. K.; Fairchild, M. N. Threading Defect Elimination in GaN Nanowires. *J. Mater. Res.* **2011**, *26*, 2293−2298.

(5) Chierchia, R.; Boettcher, T.; Heinke, H.; Einfeldt, S.; Figge, S.; Hommel, D. Microstructure of Heteroepitaxial GaN Revealed by X-ray Diffraction. *J. Appl. Phys.* **2003**, *93*, 8918−8925.

(6) Salomon, D.; Dussaigne, A.; Lafossas, M.; Durand, C.; Bougerol, C.; Ferret, P.; Eymery, J. Metal Organic Vapour-Phase Epitaxy Growth of GaN Wires on Si(111) for Light-Emitting Diode Applications. *Nanoscale Res. Lett.* **2013**, *8*, 61.

(7) Li, S. F.; Fuendling, S.; Wang, X.; Merzsch, S.; Al-Suleiman, M. A. M.; Wei, J. D.; Wehmann, H.-H.; Waag, A.; Bergbauer, W.; Strassburg, M. Polarity and Its Influence on Growth Mechanism During MOVPE Growth of GaN Sub-Micrometer Rods. *Cryst. Growth Des.* **2011**, *11*, 1573−1577.

(8) Durand, C.; Bougerol, C.; Carlin, J.-F.; Rossbach, G.; Godel, F.; Eymery, J.; Jouneau, P.-H.; Muhktarova, A.; Butté, R.; Grandjean, N. M-Plane GaN/InAlN Multiple Quantum Wells in Core-Shell Wire Structure for UV Emission. *ACS Photonics* **2014**, *1*, 38−46.

(9) Arafin, S.; Liu, X.; Mi, Z. Review of Recent Progress of III-Nitride Nanowire Lasers. *J. Nanophot.* **2013**, *7*, 074599.

(10) Tessarek, C.; Sarau, G.; Kiometzis, M.; Christiansen, S. High Quality Factor Whispering Gallery Modes from Self-Assembled Hexagonal GaN Rods Grown by Metal-Organic Vapor Phase Epitaxy. *Opt. Express* **2013**, *21*, 2733−2740.

(11) Simeonov, D.; Feltin, E.; Altoukhov, A.; Castiglia, A.; Carlin, J.-F.; Butté, R.; Grandjean, N. High Quality Nitride Based Microdisks Obtained via Selective Wet Etching of AlInN Sacrificial Layers. *Appl. Phys. Lett.* **2008**, *92*, 171102.

(12) Baek, H.; Lee, C.-H.; Chung, K.; Yi, G.-C. Epitaxial GaN Microdisk Lasers Grown on Graphene Microdots. *Nano Lett.* **2013**, *13*, 2782−2785.

(13) Tamboli, A. C.; Haberer, E. D.; Sharma, R.; Lee, K. H.; Nakamura, S.; Hu, E. L. Room-Temperature Continuous Wave Lasing in GaN/InGaN Microdisks. *Nat. Photonics* **2007**, *1*, 61−64.

(14) Simeonov, D.; Feltin, E.; Bühlmann, H.-J.; Zhu, T.; Castiglia, A.; Mosca, M.; Carlin, J.-F.; Butté, R.; Grandjean, N. Blue Lasing at Room Temperature in High Quality Factor GaN/AlInN Microdisks with InGaN Quantum Wells. *Appl. Phys. Lett.* **2007**, *90*, 061106.

(15) Aharonovich, I.; Woolf, A.; Russell, K. J.; Zhu, T.; Niu, N.; Kappers, M. J.; Oliver, R. A.; Hu, E. L. Low Threshold, Room-Temperature Microdisk Lasers in the Blue Spectral Range. *Appl. Phys. Lett.* **2013**, *103*, 021112.

(16) Dietrich, C.; Lange, M.; Böntgen, T.; Grundmann, M. The Corner Effect in Hexagonal Whispering Gallery Microresonators. *Appl. Phys. Lett.* **2012**, *101*, 141116.

(17) Tessarek, C.; Christiansen, S. Self-Catalyzed, Vertically Aligned GaN Rod-Structures by Metal-Organic Vapor Phase Epitaxy. *Phys. Status Solidi C* **2012**, *9*, 596−600.

(18) Tessarek, C.; Dieker, C.; Spiecker, E.; Christiansen, S. Growth of GaN Nanorods and Wires and Spectral Tuning of Whispering Gallery Modes in Tapered GaN Wires. *Jpn. J. Appl. Phys.* **2013**, *52*, 08JE09.

(19) Trichet, A.; Médard, F.; Zúñiga-Pérez, J.; Alloing, B.; Richard, M. From Strong to Weak Coupling Regime in a Single GaN Microwire up to Room Temperature. *New J. Phys.* **2012**, *14*, 073004.

(20) Dai, J.; Xu, C. X.; Sun, X. W. ZnO-Microrod/p-GaN Heterostructured Whispering-Gallery-Mode Microlaser Diodes. *Adv. Mater.* **2011**, *23*, 4115−4119.

(21) Grandjean, N.; Massies, J.; Leroux, M. Nitridation of Sapphire. Effect on the Optical Properties of GaN Epitaxial Overlayers. *Appl. Phys. Lett.* **1996**, *69*, 2071−2073.

(22) Chen, X. J.; Perillat-Merceroz, G.; Sam-Giao, D.; Durand, C.; Eymery, J. Homoepitaxial Growth of Catalyst-Free GaN Wires on N-Polar Substrates. *Appl. Phys. Lett.* **2010**, *97*, 151909.

(23) Li, S.; Mo, C.; Wang, L.; Xiong, C.; Peng, X.; Jiang, F.; Deng, Z.; Gong, D. The Influence of Si-Doping to the Growth Rate and Yellow Luminescence of GaN Grown by MOCVD. *J. Lumin.* **2001**, *93*, 321−326.

(24) Wang, X.; Li, S.; Fündling, S.; Wei, J.; Erenburg, M.; Wehmann, H.-H.; Waag, A. Polarity Control in 3D GaN Structures Grown by Selective Area MOVPE. *Cryst. Growth Des.* **2012**, *12*, 2552−2556.

(25) Tessarek, C.; Heilmann, M.; Butzen, E.; Haab, A.; Hardtdegen, H.; Dieker, C.; Spiecker, E.; Christiansen, S. The Role of Si During the Growth of GaN Micro- and Nanorods. *Cryst. Growth Des.* **2014**, *14*, 1486−1492.

(26) Tessarek, C.; Heilmann, M.; Christiansen, S. Whispering Gallery Modes in GaN Microdisks, Microrods and Nanorods Grown by MOVPE. *Phys. Status Solidi C* **2014**, *11*, 794−797.

(27) Coulon, P.-M.; Hugues, M.; Alloing, B.; Beraudo, E.; Leroux, M.; Zúñiga-Pérez, J. GaN Microwires as Optical Microcavities: Whispering Gallery Modes vs Fabry-Perot Modes. *Opt. Express* **2012**, *20*, 18707−18716.

(28) Grundmann, M.; Dietrich, C. P. Whispering Gallery Modes in Deformed Hexagonal Resonators. *Phys. Status Solidi B* **2012**, *249*, 871−879.

(29) Yu, G.; Wang, G.; Ishikawa, H.; Umeno, M.; Soga, T.; Egawa, T.; Watanabe, J.; Jimbo, T. Optical Properties of Wurtzite Structure GaN on Sapphire around Fundamental Absorption Edge (0.78−4.77 eV) by Spectroscopic Ellipsometry and the Optical Transmission Method. *Appl. Phys. Lett.* **1997**, *70*, 3209−3211.

(30) Foster, D. H. Fabry-Perot and Whispering Gallery Modes in Realistic Resonator Models. Ph.D. thesis, University of Oregon, Eugene, OR, 2006.

(31) Koleske, D. D.; Wickenden, A. E.; Henry, R. L.; Culbertson, J. C.; Twigg, M. E. GaN Decomposition in H-2 and N-2 at MOVPE Temperatures and Pressures. *J. Cryst. Growth* **2001**, *223*, 466−483.

(32) Reshchikov, M. A.; Morkoc, H. Luminescence Properties of Defects in GaN. *J. Appl. Phys.* **2005**, *97*, 061301.

(33) Bulutay, C.; Turgut, C. M.; Zakhleniuk, N. A. Carrier-Induced Refractive Index Change and Optical Absorption in Wurtzite InN and GaN: Full-band Approach. *Phys. Rev. B* **2010**, *81*, 155206.

(34) Wiersig, J. Hexagonal Dielectric Resonators and Microcrystal Lasers. *Phys. Rev. A* **2003**, *67*, 023807.

(35) Tchoulfian, P.; Donatini, F.; Levy, F.; Amstatt, B.; Dussaigne, A.; Ferret, P.; Bustarret, E.; Pernot, J. Thermoelectric and Micro-Raman

Measurements of Carrier Density and Mobility in Heavily Si-Doped GaN Wires. *Appl. Phys. Lett.* **2013**, *103*, 202101.

(36) Pezzagna, S.; Brault, J.; Leroux, M.; Massies, J.; de Micheli, M. Refractive Indeces and Elasto-Optic Coefficients of GaN Studied by Optical Waveguiding. *J. Appl. Phys.* **2008**, *103*, 123112.

(37) Bergmann, M. J.; Özgür, U.; Casey, H. C.; Everitt, H. O.; Muth, J. F. Ordinary and Extraordinary Refractive Indices for AlGaN Epitaxial Layers. *Appl. Phys. Lett.* **1999**, *75*, 67−69.

(38) Goldhahn, R. Dielectric Function of Nitride Semiconductors: Recent Experimental Results. *Acta Phys. Pol., A* **2003**, *104*, 123−147.

(39) Sanford, N. A.; Robins, L. H.; Davydov, A. V.; Shapiro, A.; Tsvetkov, D. V.; Dmitriev, A. V.; Keller, S.; Mishra, U. K.; DenBaars, S. P. Refractive Index Study of AlxGa1-xN Films Grown on Sapphire Substrates. *J. Appl. Phys.* **2003**, *94*, 2980−2991.

(40) Ghosh, S.; Waltereit, P.; Brandt, O.; Grahn, H. T.; Ploog, K. H. Polarization-Dependent Spectroscopy Study of M-plane GaN on LiAlO$_2$. *Appl. Phys. Lett.* **2002**, *80*, 413−415.

(41) Kouno, T.; Kishino, K.; Sakai, M. Lasing Action on Whispering Gallery Mode of Self-Organized GaN Hexagonal Microdisk Crystal Fabricatied by RF-Plasma-Assisted Molecular Beam Epitaxy. *IEEE J. Quantum Electron.* **2011**, *47*, 1565−1570.

(42) Ostwald, W. On the Assumed Isomerism of Red and Yellow Mercury Oxide and the Surface-Tension of Solid Bodies. *Z. Phys. Chem.* **1900**, *34*, 495−503.

(43) Nobis, T.; Kaidashev, E. M.; Rahm, A.; Lorenz, M.; Grundmann, M. Whispering Gallery Modes in Nanosized Dielectric Resonators with Hexagonal Cross Section. *Phys. Rev. Lett.* **2004**, *93*, 103903.

(44) Zimmler, M. A.; Capasso, F.; Müller, S.; Ronning, C. Optically Pumped Nanowire Lasers: Invited Review. *Semicond. Sci. Technol.* **2010**, *25*, 024001.

(45) Geburt, S.; Thielmann, A.; Röder, R.; Borschel, C.; McDonnnell, A.; Kozlik, M.; Kühnel, J.; Sunter, K. A.; Capasso, F.; Ronning, C. Low Threshold Room-Temperature Lasing of CdS Nanowires. *Nanotechnology* **2012**, *23*, 365204.

(46) Casperson, L. W.; Lunnam, S. D. Gaussian Modes in High Loss Laser Resonators. *Appl. Opt.* **1975**, *14*, 1193−1199.

(47) Bhowmik, A. K. Polygonal Optical Cavities. *Appl. Opt.* **2000**, *39*, 3071−3075.

(48) Gargas, D. J.; Moore, M. C.; Ni, A.; Chang, S.-W.; Zhang, Z.; Chuang, S.-L.; Yang, P. Whispering Gallery Mode Lasing from Zinc Oxide Hexagonal Nanodisks. *ACS Nano* **2010**, *4*, 3270−3276.